

Visible to shortwave infrared reflectance spectroscopy of rare earth element minerals



D. Turner^{1, a}, B. Rivard², and L. Groat¹

¹ Department of Earth, Ocean and Atmospheric Sciences, University of British Columbia, Vancouver, BC, V6T 1Z4

² Department of Earth and Atmospheric Sciences, University of Alberta, Edmonton, AB, T6G 2E3

^a corresponding author: dturmer@eos.ubc.ca

Recommended citation: Turner, D., Rivard, B., and Groat, L., 2015. Visible to shortwave infrared reflectance spectroscopy of rare earth element minerals. In: Simandl, G.J. and Neetz, M., (Eds.), Symposium on Strategic and Critical Materials Proceedings, November 13-14, 2015, Victoria, British Columbia. British Columbia Ministry of Energy and Mines, British Columbia Geological Survey Paper 2015-3, pp. 219-229.

1. Introduction

The mineralogy of rare earth element (REE) ore deposits is critical in understanding their petrogenesis but also has significant implications for metallurgy. Like many ore deposits, high-grade rocks do not necessarily equate to positive economic viability and this is especially true for REE deposits. Consequently, knowledge of sample mineralogy acquired early in a project's life can lead to more efficient exploration programs through confirmation of either 'good' or 'bad' mineralogy. Many REE minerals show fine grain sizes and their accumulation can be difficult to recognize in hand sample or drill core with an unaided eye. Knowledge of their distribution before sampling can ensure that the best rocks or core lengths are sampled for petrographic or detailed study.

REE minerals generally have complex yet diagnostic absorption patterns in visible to shortwave infrared (VNIR-SWIR) reflectance spectra that are driven primarily by REE-related $4f$ - $4f$ intraconfigurational electronic transitions. Our recent research (Turner et al., 2014, Turner 2015) has focused on three important mineral classes: REE fluorocarbonates (bastnaesite, synchysite, and parisite), REE phosphates (monazite, xenotime, and britholite), and REE-bearing silicates (cerite, mosandrite, kainosite, zircon and eudialyte). Reflectance spectra were acquired in the visible to short wave infrared regions (500 nm to 2500 nm) and samples were characterized using scanning electron microscopy and electron microprobe analysis. The results of our work and publications from other research groups (e.g., Rowan et al., 1986, Swayze et al., 2013, Hoefen et al., 2014, Boesche et al., 2015) have shown the strong applicability of reflectance spectroscopy and hyperspectral imaging to understanding, exploring, and exploiting rare earth element ore deposits and their associated rocks.

2. Background information

2.1. The lanthanides and the rare earth elements

The lanthanides (Ln) are a series of 15 elements from lanthanum (La, atomic number 57) to lutetium (Lu, atomic number 71). One of these, promethium (Pm, atomic number

61) is not naturally occurring, leaving only 14 for consideration in natural systems. The lanthanides are characterized by the presence of the $4f$ orbital block in the conventional periodic table of the elements that can accommodate 14 electrons in the seven orbital configurations. Elements of the $5f$ orbital block are known as the actinides and include uranium (U) and thorium (Th). In geological environments the lanthanides are commonly found together in their trivalent state, with the exception of divalent europium (Eu) and, in some cases, tetravalent cerium (Ce) and terbium (Tb).

Rare earth elements (REE) comprise the lanthanide group of elements, commonly yttrium (Y, atomic number 39) and sometimes scandium (Sc, atomic number 21). The two latter elements show similar non- f -block electronic structure and are locally enriched in similar rocks. The REE are commonly inconsistently subdivided by the mineral exploration industry and geoscientists into the light rare earth elements (LREE, generally La through Gd) and heavy rare earth elements (HREE, generally Tb through Lu + Y). Uncommonly a medium rare earth element (MREE) group is defined with variable identity. The lanthanides with even atomic numbers are more geologically abundant than the odd-numbered lanthanides. This gives rise to a zig-zag pattern across the REE series, which is then commonly 'removed' through normalization of REE values to C1 Chondrite concentrations.

In general, when moving from a neutral lanthanide atom with basic electronic configuration to the Ln^{3+} cation commonly found in minerals, electrons from the $4f$, $5d$ and $6s$ shells are stripped leaving a clean configuration of a sequentially occupied $4f$ orbital. At the start of the Ln series, lanthanum (La) has no unpaired $4f$ electrons (f^0), with a sequential increase of unpaired electrons (e.g., Ce and Yb as f^1 and f^3) towards gadolinium, which has seven unpaired electrons (f^7) available for electronic excitations. Lutetium (Lu), at the end of the Ln series has a filled $4f$ orbital (f^{14}) and therefore no unpaired electrons. The ionic radius of the lanthanides systematically decreases from La (largest) to Lu (smallest). The Ln^{3+} cations are generally most similar in ionic radius to U^{4+} , Th^{4+} , and Ca^{2+} . The outer radius of the $4f$ electron shells (~ 30 picometres, pm) for the

lanthanides is much less than that of the filled 5s and 5p shells (~200 pm, ~105 pm). Consequently, first assumptions suggest that the local electronic environment of Ln^{3+} cations interacts primarily with those outer shells, leaving the 4f shell relatively 'sheltered' and non-participatory in bonding.

2.2. Rare earth element minerals

In minerals, the REE predominantly populate roomy but distorted crystallographic sites with coordination numbers of eight or more. The contraction of ionic radius along the lanthanide sequence results in the heavy rare earth elements (e.g., Lu) having a greater predisposition for smaller coordination numbers (e.g., 8), whereas the larger light rare earth elements (e.g., La) prefer higher coordination numbers (e.g., 11) and longer ligand distances. This difference results in certain minerals having distinct enrichment patterns in either the light or heavy rare earths. For example, the allanite group minerals (11-coordinated, $Ln-O$ to ~3.2 Å) are LREE-enriched whereas xenotime (8-coordinated, $Ln-O$ ~2.3 Å) is defined by HREE+Y enrichment. The mineralogy of REE dominant phases can be largely ascribed to four broad mineral classes: carbonates, phosphates, silicates and oxides.

The REE carbonates mainly comprise the fluorocarbonate minerals bastnaesite, synchysite, parisite and rontgenite which all share a common stacking arrangement of $CeF-CO_3$ and $Ca-CO_3$ layers in variable ratios. Cordylite, burbankite and ancylite are REE-Ba-Sr-bearing carbonates whereas sahamalite is a REE-Mg-Fe species. Coordination of REE in these minerals is usually either 9 or 10, and mixed anion identities (e.g., O^{2-} , OH^- and F^-) are common. Consequently, bond lengths between cations and their coordinated anions vary considerably (from ~2.37 to 2.77 Å) and distortion of the coordination polyhedra is significant. REO contents for these minerals are generally high, with bastnaesite in particular showing up to ~75%.

The most common REE phosphates are monazite, xenotime and britholite. These minerals show a range of coordination states from 7 to 12 with bond lengths as short as 2.25 and as long as ~3.2 Å. Cation and anion substitutions in these minerals can be substantial with complex crystal chemical implications, such as in britholite. REO contents for these minerals are generally high and up to ~70%. Other REE bearing silicates other than those listed as examples of diverse coordinations include eudialyte, zircon, and kainosite.

The REE-bearing silicates are a diverse set of minerals with a wide range of coordination and overall crystal chemistry and structure. Coordination numbers for cation polyhedra range from 6 (gittinsite) to 11 (allanite), with some cases showing mixed anion coordination (cerite, 8 oxygen + 1 OH^-/F^-) and other minerals having more than one distinct REE site (mosandrite). Documented bond lengths vary accordingly, ranging from ~2.2 to ~3.2 Å. Crystal structures of many of the REE silicates are still not fully understood. Accordingly, REO contents for these minerals are variable and generally lower, but can be up to ~70%.

The oxide class comprises a number of different groupings

based on how the oxide is structured, the number of distinct cation sites as well as the identity and charge of the cations. The more common REE oxide minerals include fergusonite, samarskite, aeschynite, euxenite, brannerite, and loparite (e.g., Mariano and Mariano, 2012), although the list of REE-bearing oxide species is long. These minerals are commonly Fe, U and Th bearing, and metamict samples seem to be the norm rather than the exception in the literature and in mineral museums. Like the REE silicates, REO contents for these minerals are variable and generally lower, but can be up to ~60%.

2.3. Reflectance spectroscopy and hyperspectral imaging

The aim of reflectance spectroscopy is to obtain and interpret diagnostic absorption, reflection and emission properties of a target mineral (e.g., Clark, 1999). By relying on reflected light, sample preparation is greatly reduced and the analytical environments and types of potential targets are dramatically expanded, as compared to transmitted light spectroscopy commonly used by chemists in a laboratory setting. In remote sensing, spectrometers have been mounted on satellites and aircraft and used in diverse scientific applications including forest canopy, ecosystem, urban development, geologic, environmental, and planetary investigations. Hyperspectral imaging (also known as imaging spectroscopy) can be thought of as pixel-based reflectance spectroscopy where each pixel in a scene contains a spectrum. These pixels can be built up one by one via rastering of a spot spectrometer, line by line via arrays of scanning spectrometers or, more recently, as intact 'image cubes' via snapshot imaging spectrometers.

Wavelength ranges of electromagnetic energy (light) used in reflectance spectroscopy are roughly divided into ultraviolet (UV, 1 to 400 nm), visible (VIS, 400 nm to 700 nm), near infrared (NIR, 700 to 1000 nm), short wave infrared (SWIR, 1000 to 2500 nm), mid infrared (MIR, 2.5 to 8 μm) and longwave infrared (LWIR, 8 μm to 14 μm). The term VNIR (visible to near infrared) is typically from 400 nm to 1000 nm.

The interaction between electromagnetic radiation and crystalline matter results in reflection, refraction, absorption, and emission (e.g., Clark, 1999). Together, reflection and refraction define the geometrical re-distribution of photons and can be collectively termed scattering. As light passes through crystalline material it can also be absorbed by electronic and vibrational processes. The longer the ray path interacts with the target, the greater the absorption at diagnostic wavelengths from diagnostic features. When the light returns back to the spectrometer we obtain a spectrum related primarily to the nature of the material in the field of view.

Absorption bands are local attenuations of reflected light at specific wavelengths, and are generated by the target absorbing energy. The location, intensity and shape of these features can be used qualitatively and quantitatively to discern chemical and structural information about the target material (e.g., Mustard, 1992; Salisbury, 1993; Cloutis et al., 2006). In the VNIR-SWIR range, electronic and vibrational processes are the most relevant for reflectance spectroscopy of geological materials.

Electronic processes in minerals that generate absorption features in the VNIR-SWIR include crystal field effects, intervalence and metal-oxygen charge transfers, band gaps, and colour centres. Crystal field effects deal primarily with intraorbital transitions of unpaired electrons belonging to elements of the transition, lanthanide, and actinide elements. A cation with unfilled orbitals placed into a crystal field will have the energy levels of its orbitals split into lower and higher states, which allows for excitation of relaxed 'lower' electrons into higher energy levels (Fig. 1). The relative energy levels of split orbitals depend primarily on the symmetry and coordination geometry of the locally bonding ions as well as their identity (i.e., the cation-anion polyhedron; Burns, 1993). A common example of crystal field effects is the substitution of trace amounts of $^{VI}Cr^{3+}$ for $^{VI}Al^{3+}$ in corundum, leading to absorption bands centred near 420 and 550 nm (violet and green-yellow). This results in strong transmission in the 'red' region of white light and the gemstone variety known as ruby. In the mineral beryl, $^{VI}Cr^{3+}$ substituting also for $^{VI}Al^{3+}$, but in a slightly different coordination polyhedron, leads to green transmission and the gemstone variety known as emerald.

Many vibrational modes result in absorption features in the VNIR-SWIR. These features are the result of resonance between incident electromagnetic radiation and chemical bonds in minerals. In particular, the presence of water, hydroxyl and carbonate generate absorption features in the 1000 to 2500 nm through combinations and overtones of fundamental vibrations (e.g., Metal-OH bending or OH stretching) whereas the bonds between oxygen and silicon, phosphorous, and sulfur are more prominent at longer wavelengths beyond 2500 nm.

2.4. Spectroscopy of Ln^{3+} in minerals

The spectroscopic absorptions of Ln^{3+} cations in minerals are primarily the result of intraconfigurational $4f-4f$ electronic transitions. The positions and intensities of energy levels (known as Stark sublevels or multiplets) for a given lanthanide ion are governed by electrostatic, spin-orbit and crystal field interactions (e.g., Binnemans, 1996). Despite the efficient shielding of the $4f$ open orbitals by the $5s$ and $5p$ closed orbitals, the energy levels defining intraconfigurational $4f$ absorption features are not static, and subtle changes do occur depending on the specific asymmetry of the coordination polyhedron. It is this last splitting factor, the crystal field, that we are most concerned with when investigating REE-bearing minerals (e.g., Turner, 2015). The magnitude of the crystal field effects can be on the order of several hundred 100 cm^{-1} (e.g., Dieke, 1968; Fig. 2). In the VNIR range (e.g., @600 nm) this translates to positional variability of absorption bands on the order of ~ 10 nm and in the SWIR range (e.g., @2000 nm) this translates to ~ 80 nm. Generally, the greater the asymmetry of the coordination polyhedron the greater the splitting of energy levels. Similarly, a greater misfit of a Ln^{3+} cation in that coordination polyhedron will generally lead to a greater absorption coefficient. Some transitions however, are more sensitive to coordination character than others (e.g., Görrler

-Walrand and Binnemans, 1998).

Because intraconfigurational $4f-4f$ transitions require unpaired electrons in the $4f$ orbitals, not all lanthanides are spectrally active (e.g., La^{3+} , Ce^{4+} and Lu^{3+}). Compilation of Ln^{3+} absorption bands was completed by the late 1960s by Dieke et al. (1968) using high symmetry halide crystals because they best approximated a free ion state without significant crystal field effects (Fig. 3). Some of the lanthanides show hundreds of potential absorptions lines before crystal field splitting (e.g., Gd^{3+} with 327 distinct levels across 119 multiplets). For the purposes of conventional VNIR-SWIR reflectance spectroscopy however, we only consider absorptions from 4000 cm^{-1} (2500 nm) to $25,000\text{ cm}^{-1}$ (400 nm).

2.5. Principal factors influencing reflectance spectra of REE minerals

The previous sections touched briefly on the identity of the REE, the more common minerals they form, and how REE are hosted in these minerals. Basic principles of reflectance spectroscopy were presented as well as the particular electronic transitions seen in the lanthanides. Collectively, what causes the absorption features in the reflectance spectra of these REE-bearing minerals?

The most important factor is the concentration of lanthanides in a given mineral. Minerals with higher REE content will generally show stronger absorption features. In this sense, it is important to remember that many REE plots display data normalized to CI Chondrite values, not absolute concentrations. For example, even though Tm_2O_3 is commonly equally 'enriched' as neighbouring Yb_2O_3 in normalized diagrams, Yb is usually ~ 4 times greater in abundance. Therefore, even in HREE-enriched minerals Tm_2O_3 is rarely above 1 wt.% and therefore Tm^{3+} will only have very weak absorptions in the spectra of REE minerals.

Next, the coordination polyhedron of the Ln^{3+} cation and the nature of the ligands affect the specific locations of absorptions and the probability of a given intraconfigurational transition (i.e., the absorption coefficient or intensity parameters; e.g., Görrler -Walrand and Binnemans, 1998).

The actinide elements U and Th are common in many REE minerals and these elements host electrons in $5f$ orbitals. Uranium can show a variety of oxidation states but most commonly exhibits 4+ or 5+ valence charge. Absorptions related to $U^{4+,5+}$ are particularly noticeable in zircon. Thorium is most common as Th^{4+} and as such has no unpaired $5f$ electrons and therefore is not spectrally active in this respect.

Other factors that drive the overall reflectance spectra of REE minerals are those that affect other 'normal' minerals. These include crystal field effects of transition metals, charge transfers, colour centres, and conduction bands. Vibrational processes are also very important drivers of reflectance spectra (Fig. 4).

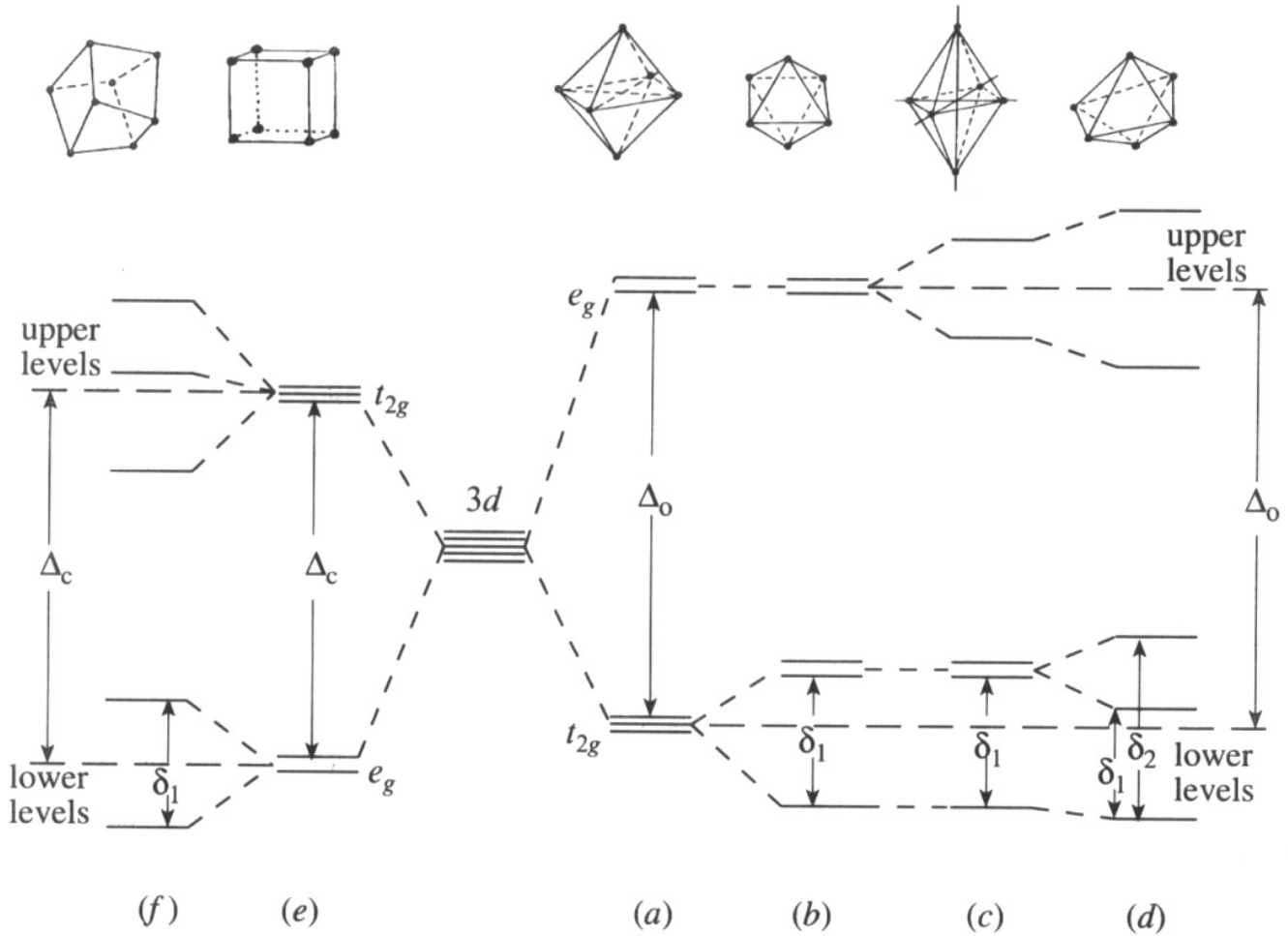


Fig. 1. Splitting of energy levels of the five *d* orbitals by cubic (e, f) and octahedral crystal fields (a – d). The Jahn Teller effect describes the subsplitting of the orbital groups by term δ , due to asymmetric distortion of a cubic environment. (From Burns 1993).

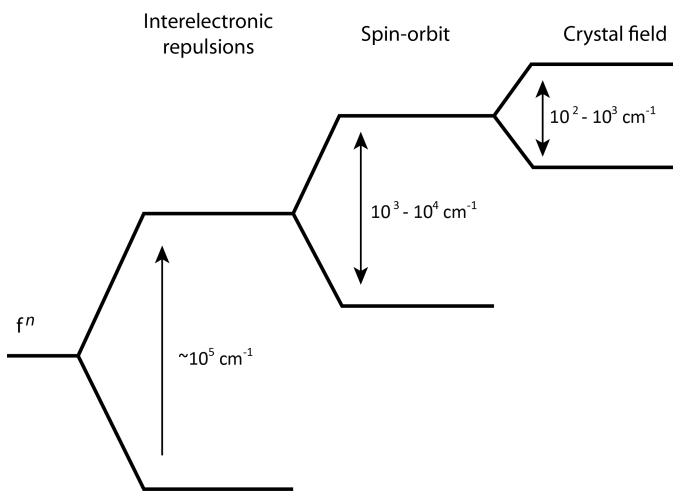


Fig. 2. Schematic representation of $4f$ energy level splitting for the lanthanides with approximate magnitudes of the splitting effects. (Modified from Malta and Carlos, 2003).

3. Examples of REE mineral reflectance spectra

3.1. The importance of REE content

The total concentration of spectrally active Ln^{3+} in a sample will impact its reflectance spectrum. Figure 5 shows 4 spectra of phosphates from the USGS Spectral Library (Speclib 06a). The pink spectrum is OH-bearing apatite lacking Ln^{3+} absorption bands whereas the red and black spectra are F- and Cl-bearing apatite with noticeable Nd^{3+} related absorptions and therefore at least trace amounts of Nd. Monazite, on the other hand, with ~60 wt.% REO, shows very strong Ln^{3+} related absorptions including Nd^{3+} at the same general location as in F and Cl bearing apatite.

Figure 6 shows reflectance spectra of four REE bearing silicates (mosandrite, cerite and 2 eudialyte samples). The plot at right shows continuum-removed spectra of the four samples and the deeper Nd^{3+} related absorptions are associated with higher Nd content. Figures 5 and 6 show that a relationship exists between the strength of at least some Ln^{3+} -related absorption bands and the concentrations of those REE in the host minerals.

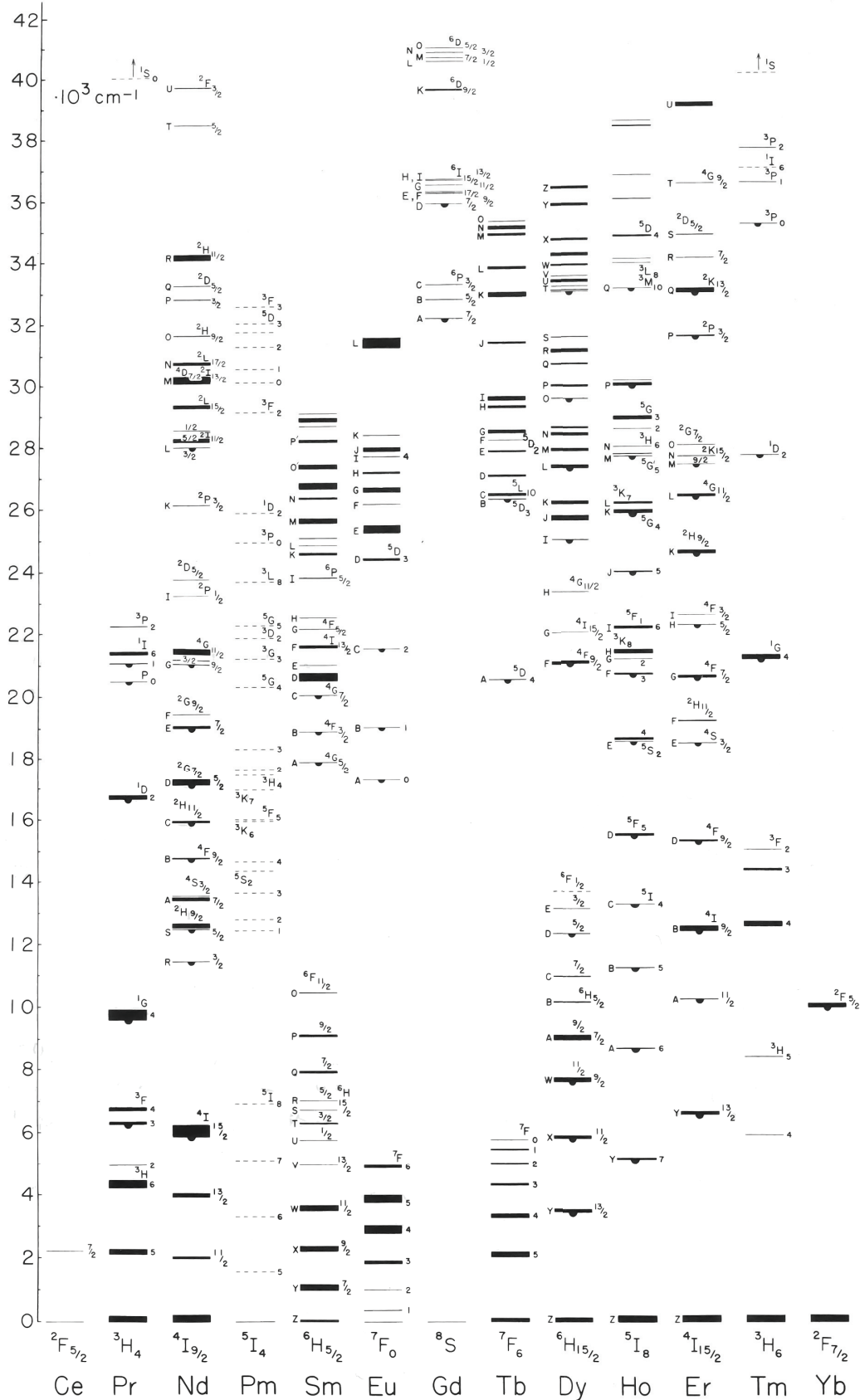


Fig. 3. 'Dieke diagram' of Ln^{3+} intraconfigurational transitions with values in $\times 1,000 \text{ cm}^{-1}$. Lines represent free ion energy levels with electron repulsion and spin-orbit interactions but before effects of a crystal field. (From Dieke et al., 1968).

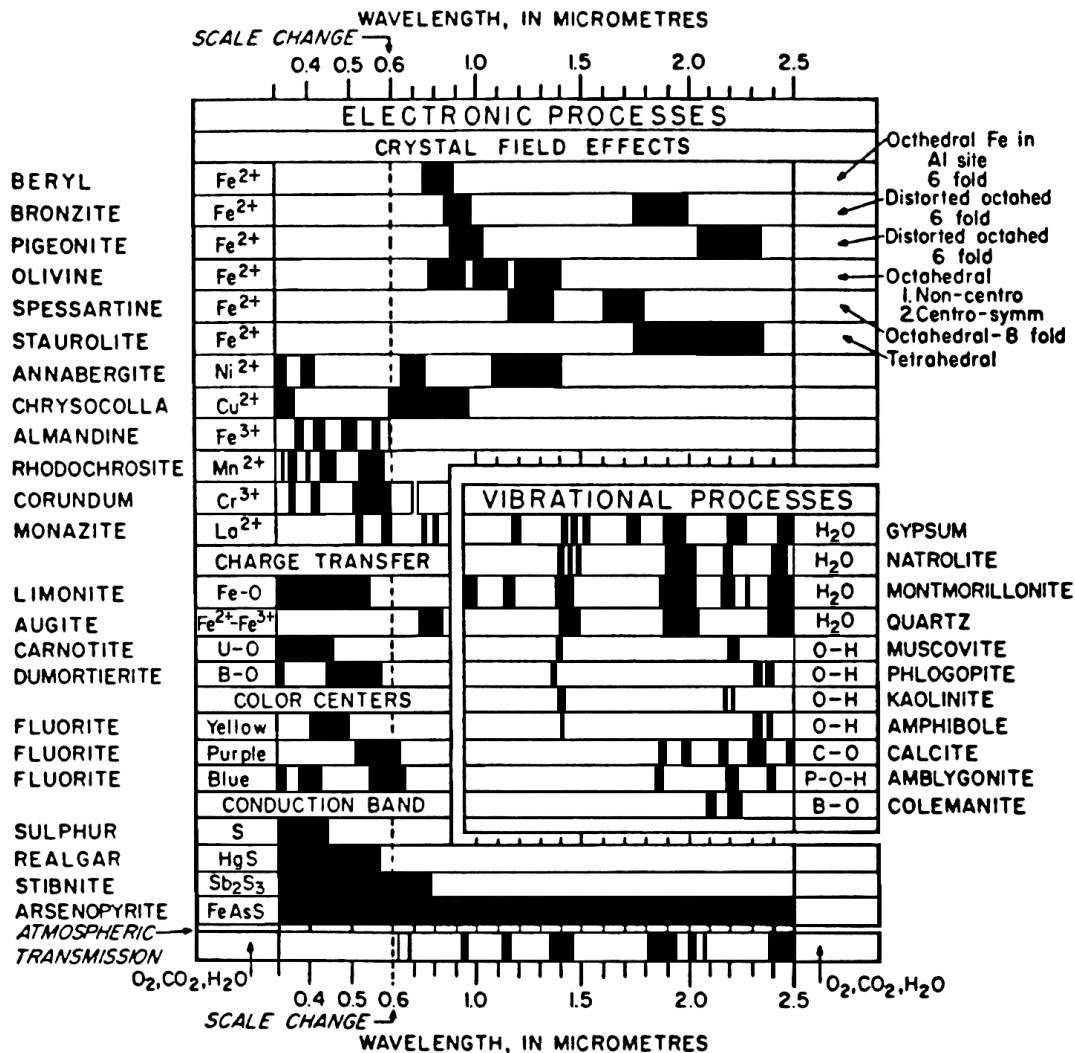


Fig. 4. Positions of diagnostic absorptions (from Hunt, 1977). Widths of black bars indicate the relative widths of absorption bands.

3.2. The importance of structure

The coordination polyhedra around Ln^{3+} can affect the positions and relative strengths of Ln^{3+} related absorptions. Figure 7 shows the coordination polyhedron of REE in parisite (a) alongside the crystal structures for bastnaesite (c, $LnCO_3F$), parisite (b, $CaLn_2(CO_3)_3F_2$) and synchysite (d, $CaLn(CO_3)_2F$). Because the site is effectively identical in each of these minerals the resulting Ln^{3+} related absorptions are also effectively identical (Figs. 8 and 9).

Conversely, coordination polyhedra that are markedly different can show significant differences in the morphology of absorptions related to the same lanthanide. For example, in Figure 6 the absorption "triplet" with bands centred near 746, 803 and 875 nm are all related to Nd^{3+} intraconfigurational electron transitions. However, it is clear that the specific locations and relative strengths of the absorption bands change depending on the coordination polyhedra of the host crystal structure. In this particular circumstance, cerite hosts three unique sites for REE that are each 9-coordinated, eudialyte

hosts two unique sites for REE that are 6 and ~9-coordinated, and mosandrite hosts REE in three unique sites that are 7 and 6-coordinated.

The relative strength of an absorption feature (i.e., the absorption coefficient) can also depend on the coordination polyhedron and how well a particular Ln^{3+} 'fits' into the existing polyhedron and structure of the mineral host, both in terms of size and valence charge. Figure 10 displays reflectance spectra of kainosite (an HREE enriched silicate with 1.56 wt.% Er_2O_3 and 1.55 wt.% Yb_2O_3) and REE-enriched zircon (with 0.16 wt.% Er_2O_3 and 0.30 wt.% Yb_2O_3). The absorption features near 978 nm are predominantly related to a Yb^{3+} transition and less so to Er^{3+} . In kainosite, $^{VIII}Ln^{3+}$ can reside at only one site, and its size parameters (expected ionic radius from structure = 1.002 Å) are well suited for the HREE, like Yb^{3+} (ionic radius of 3+ cation = 0.985 Å). In zircon Ln^{3+} substitute for $^{VIII}Zr^{4+}$ in a site that is much smaller (expected ionic radius from structure = 1.002 Å) than Yb^{3+} . We postulate that this size misfit and charge imbalance in zircon drives its stronger Yb^{3+} - Er^{3+} absorption

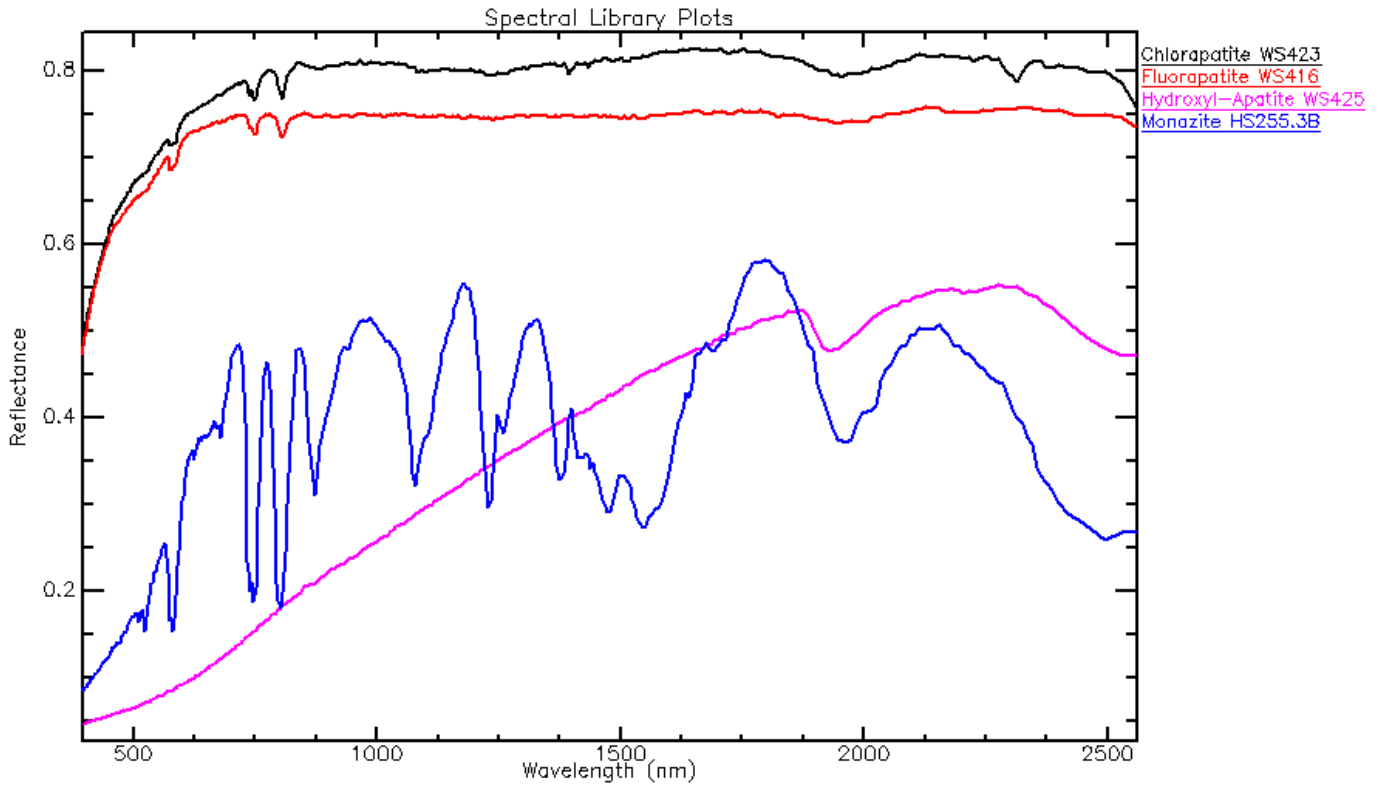


Fig. 5. Reflectance spectra from the USGS Spectral Library (Version 06a). From uppermost to lowermost near 2500 nm: Chlorapatite (black), fluorapatite (red), hydroxyl-apatite (pink) and monazite (blue). No chemical data are available.

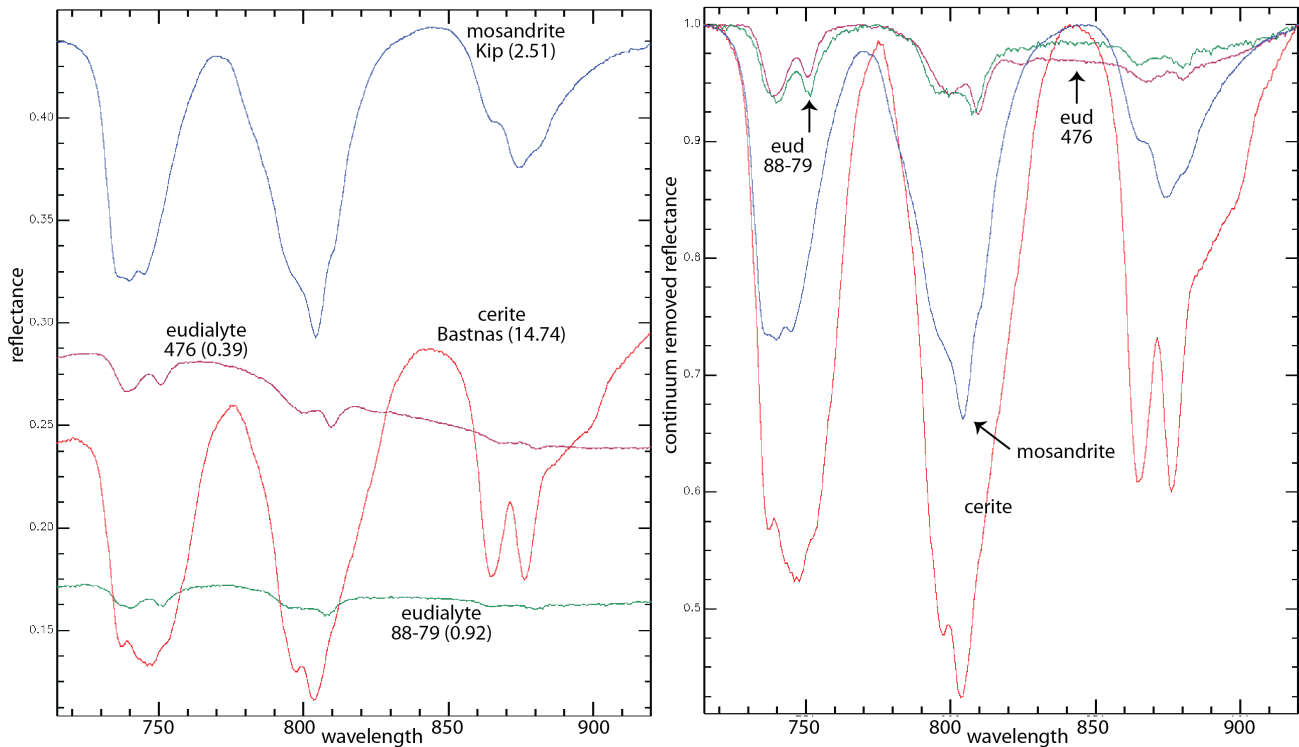


Fig. 6. Reflectance spectra (left) of selected REE bearing silicates and their continuum-removed spectra (right) displaying relative intensity and positional differences for Nd^{3+} related absorptions centred at ~ 746 nm, ~ 803 nm and 875 nm. Influence from Dy^{3+} in these samples is minimal but would be greatest in the ~ 803 nm cluster. Weight % of Nd_2O_3 for each sample is given in parentheses, as determined by electron microprobe analysis in Turner (2015).

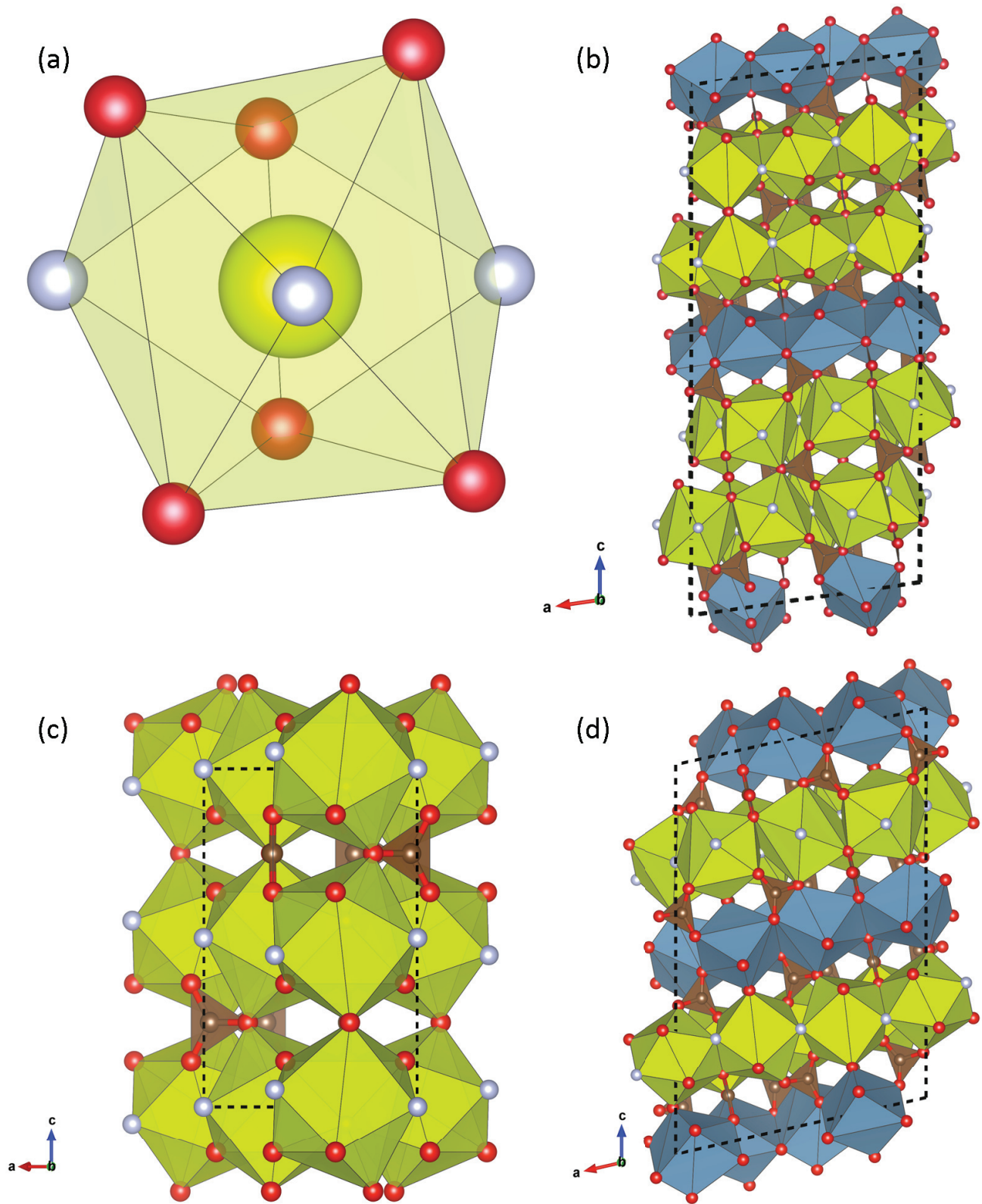


Fig. 7. **a)** Coordination polyhedron for the Ce1 site in parisite (Ni et al., 2000); also applicable to bastnaesite and synchysite. Ce1 (green) atom is coordinated with F1, F2 and F3 (lavender) atoms, whose plane is roughly perpendicular to c-axis, and 6 oxygen (red) atoms O11, O23, O32, O42, O53 and O61. Overall coordination number of 9 in a distorted tricapped trigonal prismatic arrangement. **b)** Parisite crystal structure from Ni et al. (2000). **c)** bastnaesite crystal structure from Ni et al. (1993). **d)** Synchysite crystal structure from Wang et al. (1994). Atom colouring: red=oxygen, green=REE, lavender=F, brown=C. Polyhedra colouring: green=REEO₆F₃, dark blue=CaO₈, brown=CO₃.

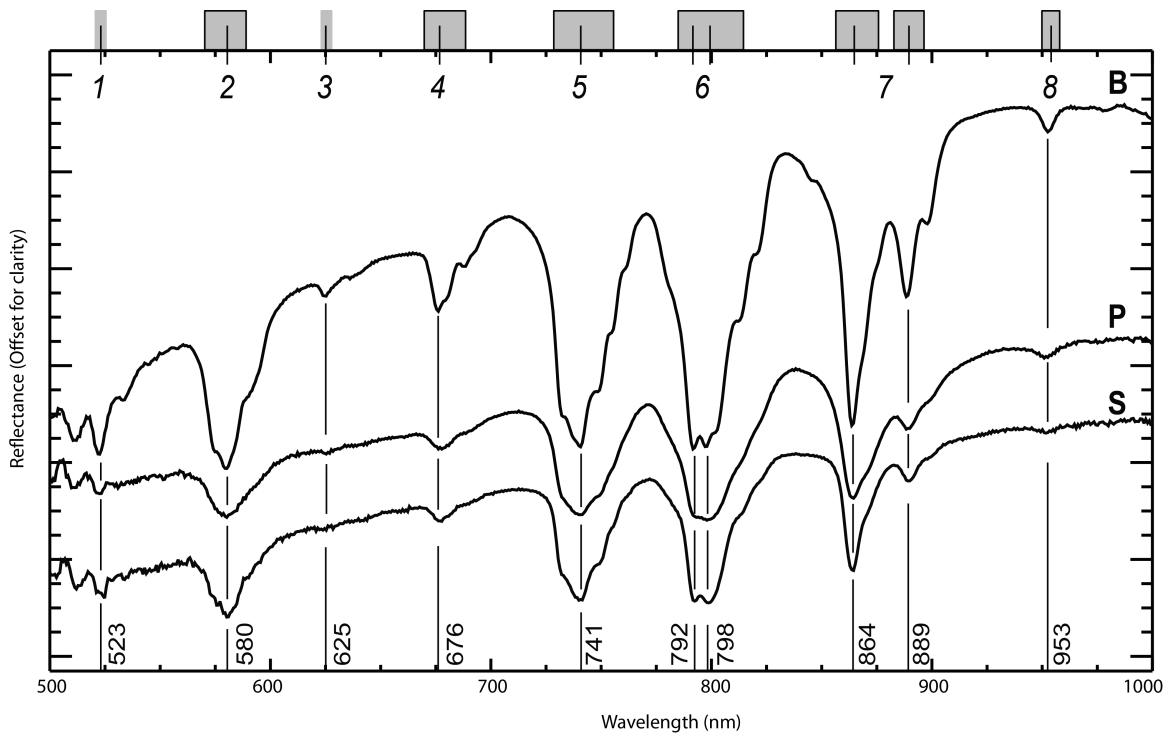


Fig. 8. VNIR (500 to 1000 nm) spectra of bastnaesite (B, top), parisite (P, middle) and synchysite (S, bottom). Italic numbers denote groups with probable origin described in Turner et al. (2014). Lines denote prominent absorption features with wavelength position, shaded boxes represent the approximate Full Width at Half Max for each absorption or absorption cluster, borderless box indicates narrow feature. Stacked spectra from sisuROCK instrument.

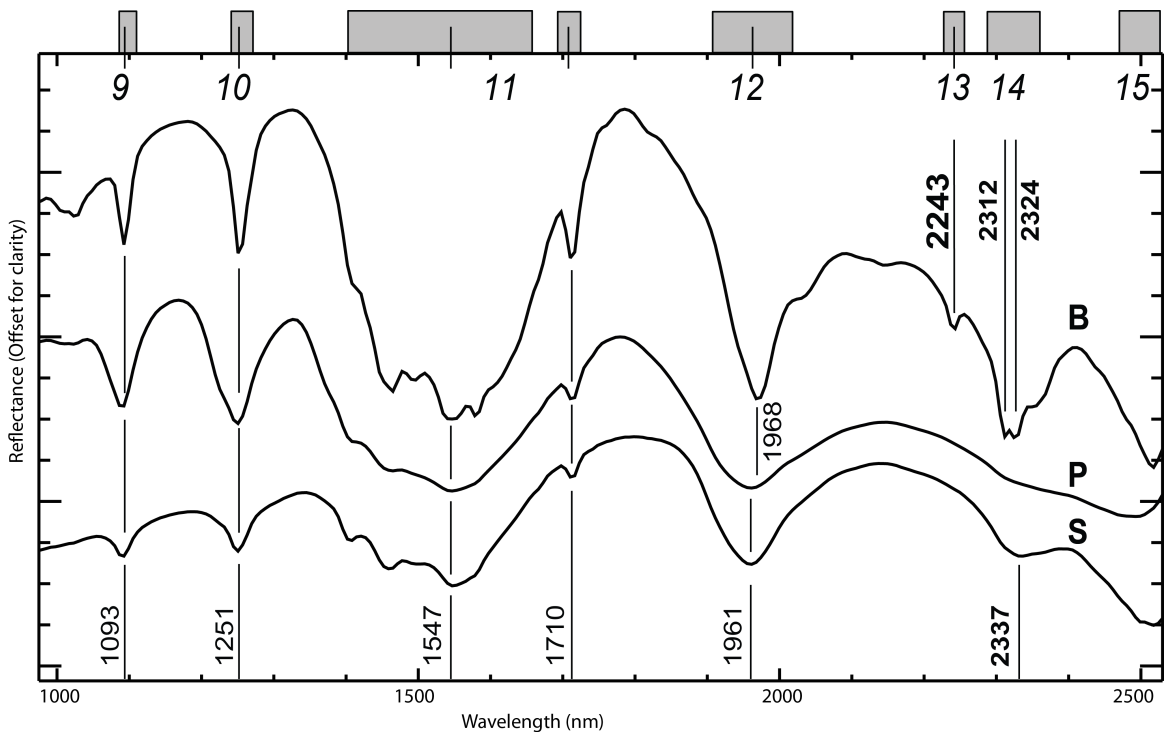


Fig. 9. SWIR (975 to 2530 nm) spectra of bastnaesite (B, top), parisite (P, middle) and synchysite (S, bottom). Italic numbers denote groups with probable origin described in Turner et al. (2014). Lines denote prominent absorption features with wavelength position, shaded boxes represent the approximate Full Width at Half Max for each absorption or absorption cluster, borderless box indicates narrow feature. Stacked spectra from sisuROCK instrument.

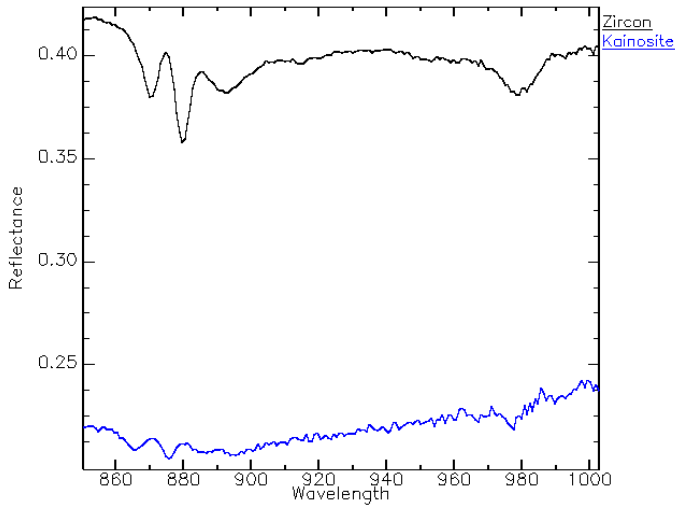


Fig. 10. Kainosite (with 1.56 wt.% Er_2O_3 and 1.55 wt.% Yb_2O_3) and REE-enriched zircon (with 0.16 wt.% Er_2O_3 and 0.30 wt.% Yb_2O_3) reflectance spectra showing the Er^{3+} - Yb^{3+} related absorption band near 978 nm.

than for kainosite, despite kainosite showing nearly an order of magnitude higher Er and Yb concentrations.

3.3. The importance of other mineral features

Despite the primary focus of this work being the Ln^{3+} related

absorption bands, all other causes of absorption features are equally important to consider and can facilitate mineral identification and discrimination based on the overall spectra. Figure 7 shows the crystal structures of the common REE fluorocarbonate minerals bastnaesite, synchysite and parisite. It was noted that the REE^{3+} coordination polyhedron was effectively identical in each mineral, however, the remainder of the structures can be thought of as being built with ‘layers’ of CeF , Ca and CO_3 in different proportions. This leads to different characteristic bonding for the various CO_3 polyhedra amongst the minerals and therefore differences in the CO_3 related vibrational absorption features in the SWIR region (Fig. 9). Specifically, a distinct absorption at 2243 nm distinguishes bastnaesite from parisite and synchysite, neither of which have this feature. Bastnaesite also shows a well resolved doublet with absorption bands at 2312 and 2324 nm, a shoulder at 2355 nm and an additional band at 2518 nm. This is in contrast to parisite’s weak absorption bands at 2324 nm and near 2499 nm, and synchysite’s absorption bands at 2337 nm and 2518 nm.

Zircon (ZrSiO_4) is a common carrier of U^{4+} and Th^{4+} and is well known to incorporate the REE^{3+} into its structure. A suite of five zircon crystals studied in detail by Turner (2015) show a range of spectral characteristics that are driven by U^{4+} , U^{5+} , a crystalline vs amorphous matrix, Ln^{3+} content and $\text{OH}/\text{H}_2\text{O}$ bands. Figure 11 displays their reflectance spectra in the VNIR

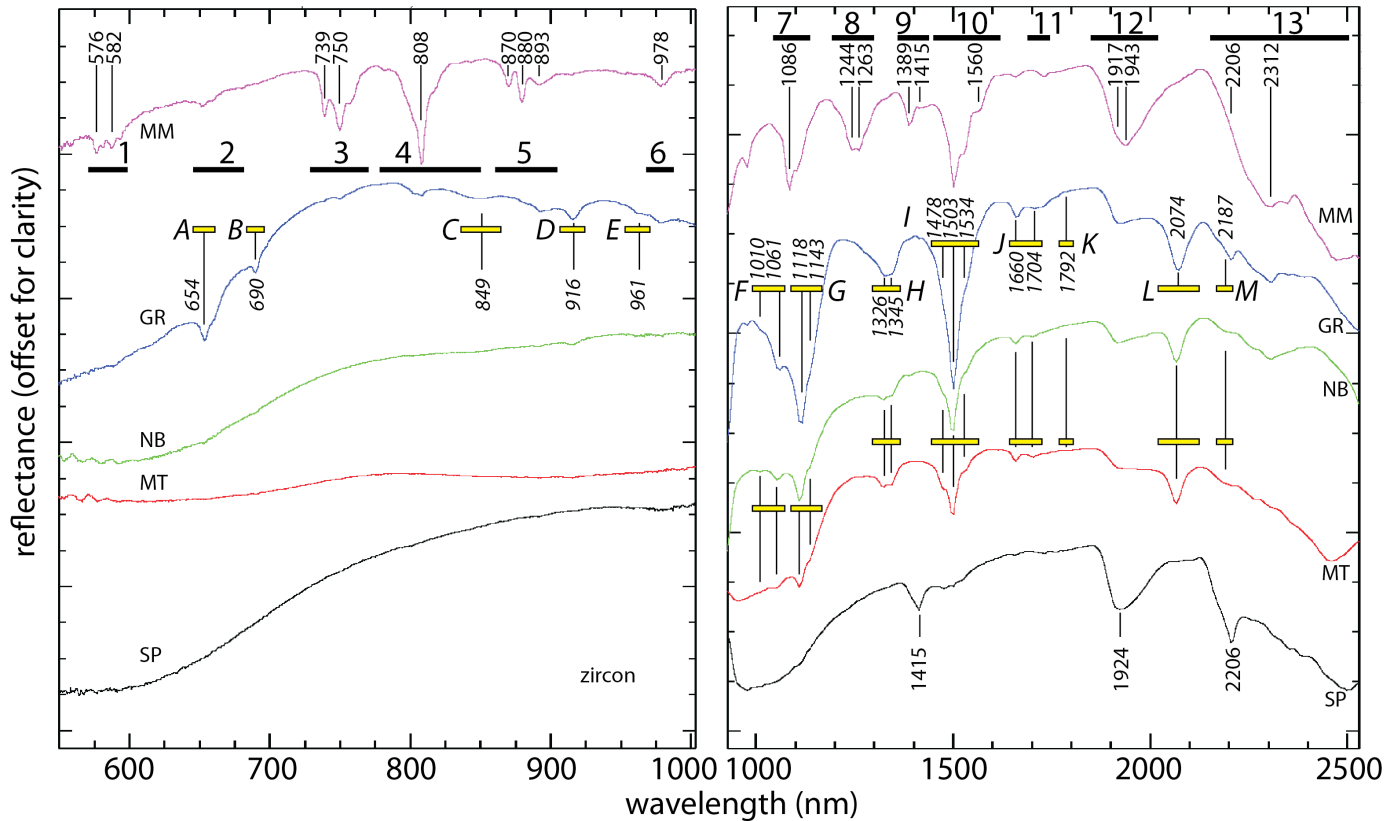


Fig. 11. Stacked reflectance spectra of zircon samples in the VNIR (550 – 1000 nm) and SWIR (975 – 2530 nm) ranges. REE-related clusters are indicated by labeled thick horizontal lines and prominent absorptions are labeled with wavelength position. Uranium related features are distinguished by lettered clusters, yellow horizontal bars and italicized wavelength labels. From top down, Mt Malosa (pink, MM) Green River (blue, GR), North Burgess (green, NB), Mudtank (red, MT), St. Peters Dome (black, SP).

and SWIR ranges, and three spectral classes of zircon exist: U bearing (North Burgess=NB, Green River=GR, Mudtank=MT), high REE with U (Mt Malosa=MM) and metamict (St Peters Dome). Many of the uranium related absorptions are fairly sharp and can overlap with regions where Ln^{3+} related absorptions are expected (e.g., the many bands near 1100 nm). This sample suite is a good example of how it is important to consider non-lanthanide variables in spectra with suspected Ln^{3+} related absorptions.

4. Conclusions and implications

Spectral features of REE minerals in the VNIR-SWIR range are primarily related to numerous $4f-4f$ intraconfigurational electronic transitions of trivalent lanthanides (Ln^{3+}), and $5f-5f$ electronic transitions of uranium and vibrational overtones and combinations of CO_3^{2-} , H_2O , and OH^- where applicable. In general, the respective spectra of the most common REE minerals are sufficiently distinct for spectral classifications. Thus, the application of reflectance spectroscopy (and especially hyperspectral imaging) can yield considerable mineralogical and geochemical information about a given REE-bearing sample. Increasing prevalence of VNIR-SWIR spectroscopy in geosciences and continuous improvement of instrumentation will no doubt benefit the understanding and exploitation of REE bearing minerals and rocks.

References cited

- Binnemans, K., 1996. A comparative spectroscopic study of Eu^{3+} in crystalline host matrices. *Bulletin des Sociétés Chimiques Belges*, 105, 793-798.
- Boesche, N. K., Rogass, C., Lubitz, C., Brell, M., Herrmann, S., Mielke, C., and Kaufmann, H., 2015. Hyperspectral REE (Rare Earth Element) Mapping of Outcrops—Applications for Neodymium Detection. *Remote Sensing*, 7, 5160-5186.
- Burns, R., 1993. *Mineralogical Applications of Crystal Field Theory*, Second Edition, Cambridge University Press, Cambridge, 551p.
- Clark, R. N., 1999. Chapter 1: Spectroscopy of Rocks and Minerals, and Principles of Spectroscopy. In: Rencz, A.N., and Ryerson, R.A., (Eds.), *Remote Sensing for the Earth Sciences, Manual of Remote Sensing Volume 3*, pp. 58.
- Cloutis, E.A., Hawthorne, F.C., Mertzman, S.A., Krenn, K., Craig, M.A., Marcino, D., Methot, M., Strong, J., Mustard, J.F., Blaney, D.L., Bell III, J.F., and Vilas, F., 2006. Detection and discrimination of sulfate minerals using reflectance spectroscopy. *Icarus*, 184, 121-157.
- Dieke, G. H., Crosswhite, H., and Crosswhite, H.M., 1968. *Spectra and energy levels of the rare earth ions in crystals*. Wiley Interscience, New York, 193p.
- Görlner-Walrand, C., and Binnemans, K., 1998. Spectral intensities of f-f transitions. In: Gschneidner, K.A., and Eyring, L., (Eds.), *Handbook on the Physics and Chemistry of Rare Earths*, Vol. 25, Chapter 167, North-Holland Publishers, Amsterdam, pp. 101-264.
- Hoefen, T. M., Livo, K. E., Giles, S. A., Lowers, H. A., Swayze, G. A., Taylor, C. D., and McCafferty, A. E., 2014. Characterization of REE-Bearing Minerals and Synthetic Materials Using High Resolution Ultraviolet to Near-Infrared Reflectance Spectroscopy. In AGU Fall Meeting Abstracts (Vol. 1, p. 4299).
- Mariano, A.N., and Mariano, A., 2012. Rare earth mining and exploration in North America. *Elements*, 8, 369-376.
- Mustard, J. F., 1992. Chemical composition of actinolite from reflectance spectra. *American Mineralogist*, 77, 345-358.
- Rowan, L. C., Kingston, M. J., and Crowley, J. K., 1986. Spectral reflectance of carbonatite and related alkalic igneous rocks from four North American localities. *Economic Geology*, 81, 857-871.
- Salisbury, J.W., 1993. Mid-infrared spectroscopy: Laboratory data. In: Pieters, C.M., and Englert, P.A.J., (Eds.), *Remote Geochemical Analysis: Elemental and Mineralogical Composition*, Cambridge University Press, Cambridge, pp. 79-98.
- Swayze, G.A., Pearson, N., Wilson, S., Benzel, W.M., Clark, R., Hoefen, T.M., Van Gosen, B., Adams, M., and Reitman, J., 2013. Spectrally distinguishing between REE-bearing minerals based on differences in their crystal field f-f transition absorptions. In Geological Society of America Abstracts with Programs, 45, 278.
- Turner, D. J., Rivard, B., and Groat, L. A., 2014. Visible and short-wave infrared reflectance spectroscopy of REE fluorocarbonates. *American Mineralogist*, 99, 1335-1346.
- Turner, D. J., 2015. Reflectance spectroscopy and imaging spectroscopy of rare earth element-bearing mineral and rock samples. Unpublished Ph.D. Thesis, University of British Columbia, Vancouver, Canada, 310p.

